American Mineralogist, Volume 92, pages 444–447, 2007

LETTER

Terrestrial analogs of martian jarosites: Major, minor element systematics and Na-K zoning in selected samples

J.J. PAPIKE,[1] P.V. BURGER,[1] J.M. KARNER,[1,*] C.K. SHEARER,[1] AND V.W. LUETH[2]

[1]Astromaterials Institute, Department of Earth and Planetary Sciences, University of New Mexico, Albuquerque, New Mexico 87131, U.S.A.
[2]New Mexico Bureau of Geology and Mineral Resources, New Mexico Institute of Mining and Technology, Socorro, New Mexico 87801, U.S.A.

ABSTRACT

Natural jarosites selected for study have mixed domains of jarosite, $KFe_3^{3+}(SO_4)_2(OH)_6$, and natrojarosite, $NaFe_3^{3+}(SO_4)_2(OH)_6$. Minor elements include Al in the octahedral B-site, and P, As, Mo, and V in the tetrahedral T-site. High abundances of As are detected in some samples. Oscillatory zoning of Na and K in a subset of these samples has been explored using BSE images, X-ray maps, and a 1 μm EDS beam. Our work shows that zoning is composed of less than micrometer-sized bands of near end-member compositions. This agrees with the XRD work of Desborough et al. (2006), where 32 natural hypogene and supergene jarosites were found to be mixtures of near end-member compositions and showed <5% solid solution. This indicates a wide solvus (miscibility gap) between jarosite and natrojarosite. It also suggests that special crystallization effects are active in solid-solution and aqueous-solution interactions. Here, the optimal conditions for the crystallization of end-member compositions are at low temperatures (<100 °C), and when the two end-members of a binary solid-solution series have different solubilities, as do jarosite and natrojarosite (Glynn 2000). These conditions are commonly found in supergene environments, and are best illustrated by spectacular oscillatory zoning of jarosite and natrojarosite in samples from the Apex Mine, Arizona and Gold Hill, Utah.

Keywords: Jarosite, Mars, zoning, terrestrial analogs, electron probe

INTRODUCTION

Jarosite is an important phase at the Meridiani locality on Mars (Klingelhöfer et al. 2004). Papike et al. (2006a, 2006b) reviewed the potential of martian jarosite as a recorder of rock-fluid interactions by using terrestrial examples. Here we discuss electron microprobe (EMP) analyses for samples from 14 selected localities. First, we discuss the chemistry of jarosite and note its potential as an indicator of potential toxins (e.g., As) on the martian surface. Second, we explore the fine-scale oscillatory zoning common in jarosite and examine how it records both the precipitation history of jarosite and fluid evolution. Last, we discuss how these insights into terrestrial jarosite formation and evolution will aid in the interpretation of robotically collected data from future missions to Mars.

SAMPLES AND ANALYTICAL TECHNIQUES

Table 1 summarizes information on the samples studied. We classify the jarosite samples as either supergene (descending solutions in the vadose zone, secondary mineralization, low-temperature, sulfur derived from alteration of preexisting sulfides) or hypogene (mostly ascending solutions, primary mineralization, higher temperatures, sulfur from oxidation of vapor species including SO_2 and H_2S). Lueth (2006) used these terms and showed how the stable isotopes of H and O can help distinguish between the two types of deposits. Sulfur isotopes encode the origin of the sulfur in jarosite (see Rye 2005), i.e., from preexisting sulfides (supergene) or from oxidation of sulfur gases (hypogene), and thus are also used to classify the samples.

The EMP analytical techniques used in this study are described in Papike et al. (2006b) and that description will not be repeated here. Before analyzing any sample we conducted a complete Wavelength Dispersive Spectrometry (WDS) scan to see which elements were detectable by EMP. All analyses were first normalized to 14 O atoms and then to 2.00 tetrahedral cations per formula unit; all Fe is reported as 3+. The average compositions for the 14 samples are presented in Table 2. We note that in Papike et al. (2006b) we provided formulae for specific analyses, but here we do not. The reason for this is that many of these samples consist of microcrystalline matted fibers, which are difficult to analyze. Vapor loss is a significant problem and required us to use a broad beam size of 30 μm, so most analyses are bulk values from several crystals. Therefore the data in Table 2 are presented in the most defensible manner. In Papike et al. (2006a) we discuss various charge-balance couples that may be important in jarosite. For example, the substitution of P^{5+} or V^{5+} for S^{6+} in the jarosite tetrahedral site requires a charge balance. We believe the most important charge balancing cation in these samples is Pb^{2+} in the A-site but we do not report Pb data here. This is because fine-grained galena (PbS) is suspected to contribute to high Pb concentrations in some broad beam analyses. Lastly, we found no evidence for significant substitution of the hydronium ion (H_3O^+) into the A-site of jarosite. Significant hydronium substitution would have shown up as totals less than 1.00 for the sum of A-site cations.

RESULTS AND DISCUSSION

Chemical variation in jarosite for Na, K, Al, Fe^{3+}, S, P, As, Mo, and V by broad beam WDS analysis

Variation of Na/(Na + K) (atomic) in the 12-coordinated A-site is illustrated in Figure 1a and variation of Al/(Al + Fe^{3+}) (atomic) in the octahedral B-site is illustrated in Figure 1b. Several interesting observations can be made by studying these plots. First, a large variation in Na/(Na + K) (atomic) reflects a large variation of Na and K in the aqueous fluids. For example, the Peña Blanca jarosite (sample 14) shows that the solutions from which it formed had essentially no Na. A second observation is that the broad beam analyses give the impression of significant preserved solid solution between jarosite and natrojarosite. This is not actually the case and will be discussed in more detail in the following section. Another observation is that Al/(Al + Fe^{3+}) also shows a large variation in the jarosites, but over a much smaller

* E-mail: jkarner@unm.edu

TABLE 1. Jarosite sample information

Sample no.	Classification	Locality	Texture	Comments	References
1	Hypogene	Mina La Mojina, Mexico	Massive, platy to fibrous	With skarn or replacement strata-bound ore mineralization	Lueth et al. 2005
2	Hypogene	Post Pit, NV	Euhedral crystals on shale	With strata-bound gold mineralization	
3	Supergene	Apex Mine, AZ	Vein fill, euhedral crystals	Supergene destruction of porphyry copper deposits	
4	Supergene	Gold Hill, UT	Vein fill, subhedral crystals	Occurs on brecciated gossan from the glory hole of the mine	Kokinos and Wise 1993
5	Uncertain	Almeiria, Spain	Euhedral crystals on hematite	Stable isotopes not determined	Martinez-Frías et al. 2004
6 7	Supergene	Gumma Iron Mine, Japan	Massive, granular	With goethite from modern warm springs	Akai et al. 1997; Lueth et al 2005
8	Supergene	Morenci Mine, AZ	Euhedral crystals on quartzite	Supergene destruction of porphyry copper deposits	Enders 2002
9	Hypogene	Copiapo Mine, NM	Massive, fibrous	All occur in limestone-hosted	Lueth et al. 2005
10	Hypogene	Sunshine Mine, NM	Fracture fill	barite, fluorite, galena deposits.	
11	Hypogene	Sandia Crest, NM	Matted fibers	Jarosite occurs late ± fluorite	
12	Hypogene	Bluestar Mine, NM	Fibrous crystals on fluorite		
13	Hypogene	Goldfield, NV	Crystal overgrowths on alunite	Breccia fillings in trachyandesite and rhyodacite flows	Keith et al. 1979; Papike et al. 2006a, 2006b
14	Hypogene	Peña Blanca, Mexico	Euhedral crystals	In rhyolite breccia with fluorite	Lueth et al. 2005

TABLE 2. Summary of jarosite chemistry (averages) as determined by the electron microprobe

Sample	1	2	3	4	5	6	7	8	9	10	11	12	13	14
No. of Analyses	24	30	17	15	30	20	20	30	20	10	30	30	17	18
Cations based on 14 O atoms (Papike et al. 2006b) and T = 2.00														
A-site														
Na/Na + K (atomic)	0.06	0.01	0.20	0.07	0.05	0.02	0.02	0.05	0.25	0.08	0.77	0.09	0.43	0.00
B-site														
Al/Al + Fe^{3+} (atomic)	0.00	0.02	0.00	0.00	0.02	0.01	0.01	0.07	0.00	0.01	0.00	0.00	0.04	0.05
T-site (afu)														
S	1.94	1.94	1.99	2.00	2.00	1.95	1.94	1.99	2.00	1.97	1.97	1.96	1.98	1.98
P	0.00	0.02	0.00	0.00	0.00	0.03	0.05	0.01	0.00	0.03	0.00	0.02	0.01	0.00
V	0.00	0.03	0.00	0.00	0.00	0.01	0.00	0.00	0.00	0.00	0.00	0.00	N/A	0.00
As	0.06	0.01	0.01	0.00	0.00	0.01	0.01	0.00	0.00	0.00	0.03	0.02	0.01	0.01
Mo	0.00	0.00	0.00	0.00	0.00	0.00	0.00	0.00	0.00	0.00	0.00	0.00	0.00	0.01
Sum = 2.00	2.00	2.00	2.00	2.00	2.00	2.00	2.00	2.00	2.00	2.00	2.00	2.00	2.00	2.00
T-site (ppm, wt.)														
P	b.d.	1119	246	166	b.d.	1884	2439	681	125	1591	b.d.	488	283	b.d.
V	b.d.	2980	b.d.	b.d.	b.d.	489	b.d.	b.d.	b.d.	b.d.	b.d.	b.d.	N/A	b.d.
As	8141	1922	1313	b.d.	b.d.	1191	b.d.	b.d.	b.d.	b.d.	4859	1696	1075	1541
Mo	b.d.	b.d.	b.d.	b.d.	b.d.	b.d.	b.d.	b.d.	b.d.	b.d.	b.d.	b.d.	b.d.	1252

Notes: b.d. = below detection. Detection limit is 3 times the counting statistic standard deviation at a 99% confidence level. N/A = Not analyzed. Electron microprobe values have typical errors of 3% for major elements and up to 5% for minor and trace elements.

interval (0 to 15 mol%) than Na/(Na + K) (0 to >90 mol%). This is basically what Papike et al. (2006b) described for the Goldfield, Nevada, jarosite. Also, there is no apparent correlation of Na/(Na + K) with Al/(Al + Fe^{3+}).

Figure 2 illustrates the variation of P, V, As, and Mo in the tetrahedral site of jarosite. Note the high abundances of As in sample 1 (Mina la Mojina, Mexico), the high abundance of Mo in sample 14 (Peña Blanca, Mexico), and the high abundance of V in sample 2 (Post Pit, Nevada). A conservative estimate of the detection limits of these elements by EMP WDS techniques is shown in Table 2. In Figure 2, however, we show the complete range of concentrations we obtained, fully realizing that low abundances have large errors associated with them.

Na-K systematics

Here we explore fine-scale Na-K zoning in the samples to constrain the conditions of jarosite growth. The Na-K zoning was characterized using a combination of back-scattered electron (BSE) imaging, X-ray mapping, and quantitative Energy Dispersive Spectrometry (EDS) analysis (1 μm beam). BSE imaging of the 14 jarosite samples from various terrestrial environments reveals a range in zoning development, from samples with no visible zoning to those with spectacular oscillatory bands (samples 3 and 4), as shown in Figure 3. Differences in zoning among these samples is likely due to temperature of crystallization, crystallization kinetics, nucleation energetics, crystal growth mechanisms, and fluid chemistry. In samples 3 and 4, jarosite growth begins with multiple nucleation sites, leading to the growth of numerous euhedral crystals (Fig. 3a), possibly when an oxidant is introduced into the system (Papike et al. 2006b). X-ray maps and EMP analyses confirm that the zoning bands are defined by fluctuations in Na and K, while Al and Fe show little or no variation. Na-K zoning is likely caused by changes in Na and K concentration in the fluid immediately adjacent to zones of crystal growth. The reason for these changes will be discussed below. In the case of sample 3, Apex Mine, Arizona (Figs. 3a and 3b), later precipitation/crystal growth is characterized by a higher concentration of Na and lower K, suggesting

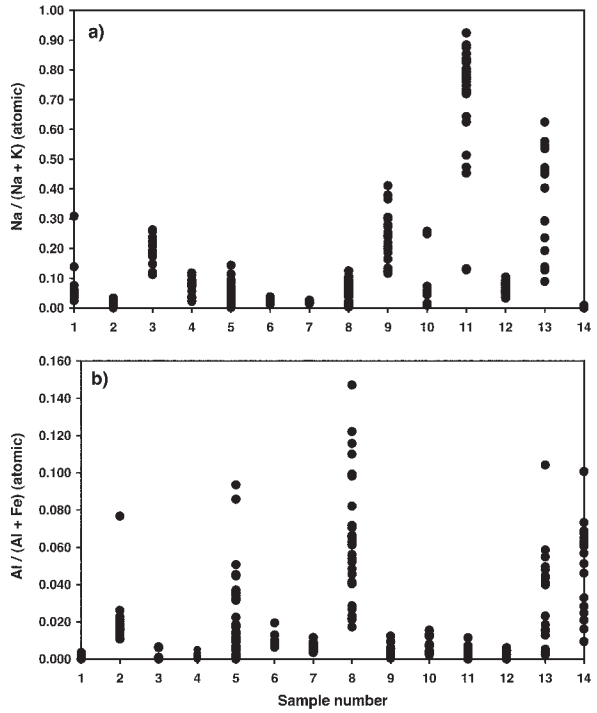

FIGURE 1. (**a**) Na/(Na + K) (atomic) systematics and (**b**) Al/(Al + Fe^{3+}) (atomic) systematics for the 14 jarosite samples. See text for discussion.

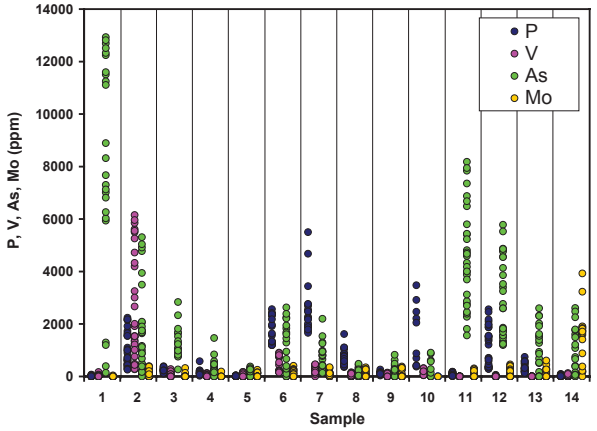

FIGURE 2. Range of concentrations (ppm by wt.) of P, V, As, and Mo in the tetrahedral site of jarosite for the 14 samples. See text for discussion.

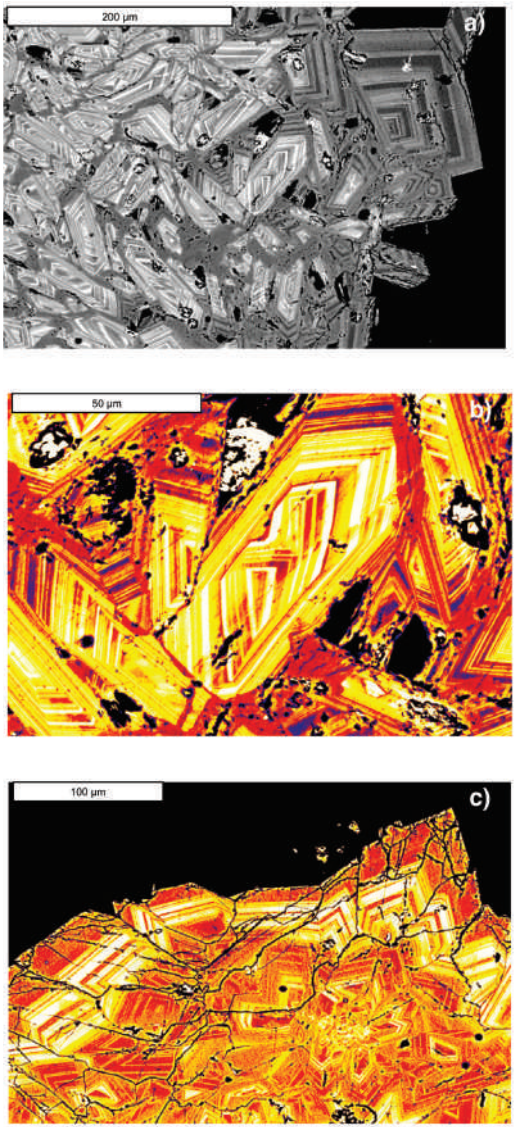

FIGURE 3. (**a**) BSE image of jarosite crystals with prominent oscillatory zoning in sample 3 (Apex Mine, Arizona). Darker regions are more sodic. (**b**) False-color BSE image of jarosite crystals in sample 3. Later (outer), redder regions are more sodic. (**c**) False-color BSE image of jarosite sample 4 (Gold Hill, Utah). See text for discussion.

the overall fluid composition has become more sodic. Further growth likely results in coalescing of various crystals, as voids are filled. Sample 4, Gold Hill, Utah (Fig. 3c), may represent this later stage of crystal growth, as it appears that there were once numerous crystals and now one large grain has developed. Subsequent crystal growth is characterized by zoning along the periphery of the large grain, the area to which fluids were likely sequestered once voids between crystals had been filled in. While zoning is quite dramatic in BSE images, EMP analyses (Table 2) suggest that the overall Na/(Na + K) in samples 3 and 4 is quite low when compared to sample 13 (Goldfield, Nevada), as discussed in Papike et al. 2006b. From our broad beam WDS analyses, it seems the zoning in samples 3 and 4 is made up of intermediate compositions between jarosite and natrojarosite. Note, however, that Desborough et al. (2006) studied 32 natural hypogene and supergene K- and Na- jarosites by XRD and found them to be mixtures of near end-member compositions with <5% solid solution. This indicates a wide solvus (miscibility gap). Contrary to our broad beam WDS analyses, our EDS analyses (1 µm beam) agree with this conclusion of limited miscibility. This is illustrated in an EDS traverse from the center to the edge of a growing crystal (Fig. 4). We propose that at low temperature conditions with rapid crystallization, compositions within the jarosite-natrojarosite solvus (miscibility gap) will not crystallize.

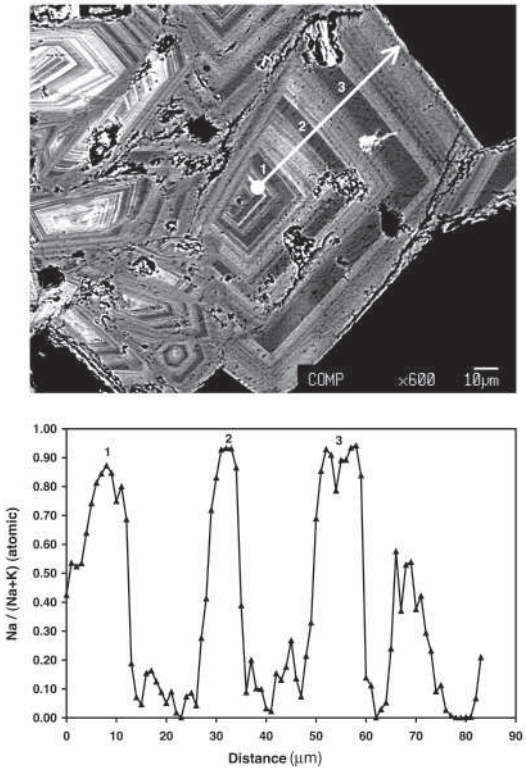

FIGURE 4. BSE image magnifying the upper right corner of Figure 3a, and corresponding plot of EDS traverse (1 µm beam). The plot shows the traverse with respect to Na/(Na + K) (atomic) and denotes the composition of bands 1, 2, and 3, that correspond to the image.

Furthermore, instead of forming an equilibrium pair of (near) end-member phases on both sides of the solvus, we form the two phases sequentially, one nucleating on the other and sharing a common surface. Thus, the composition jumps back and forth across the solvus like a ping-pong ball. An additional way this zoning could form is to grow the crystal in a direction parallel to the K and Na layers, so that the two phases grow together but share common surfaces (epitaxy). Presently we are studying the oscillatory zoned samples by Transmission Electron Microscopy (TEM) to explain the origin of the two phases. The combination of high resolution TEM imaging, electron diffraction, and EDS will allow us to define the zoning mechanism as either (1) growth phenomena and epitaxy during crystallization; or (2) exsolution, which involves post-crystallization phase separation on an optimal phase boundary, likely quite distinct from the orientation of the crystal growth surfaces.

The reasons for this type of crystallization are rigorously discussed by Glynn (2000). He shows that in low temperature (<100 °C) systems, where the two end-members have different solubilities, as between jarosite (lower) and natrojarosite (higher), alternate bands of the two phases are to be expected. Such systems are controlled by the least soluble end-member, jarosite in this case.

These effects should be most common in supergene deposits (e.g., Apex Mine, Arizona, and Gold Hill, Utah). However, we have also found similar crystallization effects in jarosite from the hypogene deposit in Goldfield, Nevada, where temperatures were estimated at approximately 200 °C and the timing of the alunite-jarosite crystallization and mineralization were the same (Papike et al. 2006b).

Implications for the 2009 Mars Science Laboratory (MSL) Mission

The results reported here, and those of Desborough et al. (2006) and Glynn (2000), have important implications for the use of the combined XRD/XRF (CheMin) instrument on the 2009 MSL mission. See Papike et al. (2006a) for a brief discussion. The X-ray diffraction analysis of martian jarosite will likely show two patterns (i.e., natrojarosite and jarosite). Although this is pushing the XRD on CheMin to the limit (D. Vaniman, pers. comm.) the CheMin flight instrument is well advanced and has solved the difficulties of preferred orientation of grains and makes full use of both diffraction peak intensity and position to obtain quantitative abundance data. Hopefully, the modal abundance of these two domains within the jarosite can then be determined and recombined to obtain the average crystal composition within the natrojarosite-jarosite miscibility gap.

ACKNOWLEDGMENTS

We sincerely thank Mike Spilde for his help with the EMP analyses. Reviews by D.C. Golden and David Vaniman significantly improved the manuscript. A NASA Cosmochemistry Grant to J.J.P. supports this research, which we gratefully acknowledge.

REFERENCES CITED

Akai, J., Kawamoto, K., Akai, K., and Nakano, S. (1997) Biogenic contribution to the formation of iron ore in Gumma Iron Mine, central Japan. Proceedings of the 30th International Geology Congress, 9, 199–208.

Desborough, G.A., Smith, K.S., Lowers, H.A., Swayze, G.A., Hammarstrom, J.A., Diehl, S.F., Driscoll, R.L., and Leinz, R.W. (2006) The use of synthetic jarosite as an analog for natural jarosite. Proceedings of the 7th International Conference on Acid Rock Drainage (ICARD), 458–475.

Enders, S.M. (2002) The evolution of supergene enrichment in the Morenci porphyry copper deposit, Greenlee County, Arizona, 517 p. Ph.D. dissertation (unpublished), University of Arizona.

Glynn, P. (2000) Solid-solution solubilities and thermodynamics: Sulfates, carbonates, and halides. In C.N. Alpers, J.L. Jambor, and D.K. Nordstrom, Eds., Sulfate Minerals, 40, p. 481–511. Reviews in Mineralogy and Geochemistry, Mineralogical Society of America, Chantilly, Virginia.

Keith, W.J., Calk, L., and Ashley, R.P. (1979) Crystals of coexisting alunite and jarosite, Goldfield, Nevada. Shorter contributions to mineralogy and petrology. U.S. Geological Survey Professional Paper 1124-C, C1–C5.

Klingelhöfer, G., Morris, R.V., Bernhardt, B., Shröder, C., Rodinov, D.S., de Souza, P.A., Yen, A., Gellert, R., Evlanov, E.N., Zubkov, B., Foh, J., Bonnes, U., Kankeleit, E., Gütlich, P., Ming, D.W., Renz, F., Wdowiak, T., Squyres, S.W., and Arvidson, R.E. (2004) Jarosite and hematite at Meridiani Planum from Opportunity's Mössbauer spectrometer. Science, 306, 1740–1745.

Kokinos, M. and Wise, W.S. (1993) The Gold Hill mine, Tooele County, Utah. Mineralogical Record, 24, 11–22.

Lueth, V.W. (2006) Textural and stable isotope discrimination of hypogene and supergene jarosite and environment of formation effects on $^{40}Ar/^{39}Ar$ geochronology (abstract). Martian Sulfates as Recorders of Atmospheric-Fluid-Rock Interactions workshop, LPI contribution XXX. Lunar and Planetary Institute, Houston, Texas.

Lueth, V.W., Rye, R.O., and Peters, L. (2005) "Sour gas" hydrothermal jarosite: ancient to modern acid-sulfate mineralization in the southern Rio Grande Rift. Chemical Geology, 215, 339–360.

Martinez-Frías, J., Lunar, R., Rodríguez-Losada, J.A., Delgado, A., and Rull, F. (2004) The volcanism-related multistage hydrothermal system of El Jaroso (SE Spain): Implications for the exploration of Mars. Earth Planets Space, 56, 5–8.

Papike, J.J., Karner, J.M., and Shearer, C.K. (2006a) Comparative planetary mineralogy: Implications of martian and terrestrial jarosite. A crystal chemical perspective. Geochimica et Cosmochimica Acta, 70, 1309–1321.

Papike, J.J., Karner, J.M., Spilde, M.N., and Shearer, C.K. (2006b) Terrerestrial analogs of martian sulfates: Major and minor element systematics of alunite–jarosite from Goldfield, Nevada. American Mineralogist, 91, 1197–1200.

Rye, R.O. (2005) A review of stable-isotope geochemistry of sulfate minerals in selected igneous environments and related hydrothermal systems. Chemical Geology, 215, 5–36.

MANUSCRIPT RECEIVED SEPTEMBER 1, 2006
MANUSCRIPT ACCEPTED SEPTEMBER 21, 2006
MANUSCRIPT HANDLED BY BRYAN CHAKOUMAKOS